Optical properties of mineral dust outbreaks over the northeastern Mediterranean

Nilgün Kubilay, Tulay Cokacar, and Temel Oguz
Institute of Marine Sciences, Middle East Technical University, Erdemli, Turkey

Received 23 May 2003; revised 21 July 2003; accepted 7 August 2003; published 6 November 2003.

[1] Ground-based aerosol optical measurements were conducted within the framework of the Aerosol Robotic Network (AERONET) program at the IMS-METU site at Erdemli (36°33′N, 34°15′E) along the Turkish coast of the northeastern Mediterranean from January 2000 to June 2001. The measurements were used to identify and define predominant regional aerosol optical properties, with an emphasis on mineral dust intrusion events. Dust storms affecting the region primarily originate from the central Sahara in spring, the eastern Sahara in summer, and the Middle East/Arabian peninsula in autumn. Summer and autumn dust intrusions usually occurred at higher altitudes (above 700 hPa), whereas urban-industrial aerosols from the north over the Balkan region, Ukraine, and Anatolia were transported to the region at lower altitudes. In addition to a drastic increase in the aerosol optical thickness, in some cases up to 1.8, the dust episodes were characterized by (1) a sharp drop in the Ångstrom coefficient to values near zero, (2) a high-scattering with single-scattering albedo greater than 0.95 ± 0.03, and the real part of the refractive index around 1.5 ± 0.5, both of which acquire slightly higher values at longer wavelengths, (3) a lower absorption given by the imaginary part of the refractive index less than 0.002, and (4) an almost neutral spectral dependence of these parameters. Dust particles possessed a bimodal size distribution with typical volume mean radii of 2.2 μm and 0.08 μm for coarse and fine size fractions, respectively, and corresponding volume concentrations of about 1.0 and 0.1 $\mu m^3\ \mu m^{-2}$ of dust particles. It was apparent that the Saharan and Middle East desert dusts differ in their absorption index values (0.0015 and 0.0005, respectively). The difference is likely a result of their contrasting mineralogies. *INDEX TERMS:* 0305 Atmospheric Composition and Structure: Aerosols and particles (0345, 4801); 0365 Atmospheric Composition and Structure: Troposphere—composition and chemistry; 0368 Atmospheric Composition and Structure: Troposphere—constituent transport and chemistry; 3360 Meteorology and Atmospheric Dynamics: Remote sensing; *KEYWORDS:* aerosols, eastern Mediterranean, optical properties

Citation: Kubilay, N., T. Cokacar, and T. Oguz, Optical properties of mineral dust outbreaks over the northeastern Mediterranean, *J. Geophys. Res.*, *108*(D21), 4666, doi:10.1029/2003JD003798, 2003.

1. Introduction

[2] Atmospheric aerosols from both anthropogenic (e.g., sulfate, biomass burning smoke, black carbon) and natural sources (e.g., mineral dust and sea salt) introduce large temporal and regional variabilities in the heat balance of the Earth by (i) scattering and absorbing solar radiation, (ii) absorbing and emitting some terrestrial infrared radiation, and (iii) their ability to nucleate cloud droplets [*Kaufman et al.*, 2002a, and references therein]. The global radiative forcing due to aerosols is roughly $-1.6 \pm 1.3\ Wm^{-2}$, which nearly compensates the mean global radiative forcing of $2.4 \pm 0.3\ Wm^{-2}$ due to greenhouse gase warming [*Intergovernmental Panel on Climate Change*, 2001]. The way in which these effects are considered using observed data in climate models and remotely sensed ocean color algorithms is fundamentally important for the understanding of long-term impacts of aerosols on future climate change, and the retrival of more realistic ocean bio-optical products [*Gao et al.*, 2001; *Moulin et al.*, 2001a]. Even though global-scale monitoring programs, recently initiated using a surface-based network of observations [*Holben et al.*, 1998], have improved our knowledge on aerosol optical properties, aerosol forcing is still poorly defined in climate change simulations [*Tegen et al.*, 1996; *Heintzenberg et al.*, 1997; *Hansen et al.*, 2000] as well as in the scope and accuracy of satellite remote sensing products [*Kaufman et al.*, 1997; *King et al.*, 1999]. For example, the standard SeaWiFS algorithm fails to retrieve chlorophyll concentrations and aerosol optical properties during dust events having aerosol optical thickness values greater than 0.3. The corresponding pixels are discarded in the processing procedure [*Wang et al.*, 2000]. In particular the Mediterranean atmosphere, often loaded by Saharan desert dust from the south and by urban and anthropogenic-based aerosols

0148-0227/03/2003JD003798$09.00

derived from the continental landmass to the north, offers a challenge in terms of filtering the enhanced absorption in the blue and the enhanced backscattering in the green parts of visible spectrum with respect to their background values in the absence of dust outbreak events [*Claustre et al.*, 2002].

[3] The global Aerosol Robotic Network (AERONET) operated by the NASA Goddard Space Flight Center [*Holben et al.*, 1998, 2001] has been collecting near-real time data over 100 sites covering many climatically important regions worldwide for almost a decade. Ground-based measurements involve the collection of spectral data of direct Sun radiation extinction (i.e., aerosol optical thickness), and angular distribution of sky radiance, the combination of which allows retrieval of various aerosol optical properties using an inversion algorithm [*Dubovik and King*, 2000]. These data began to provide systematic identification of globally distinct aerosol optical characteristics, representing biomass burning, urban, oceanic and desert sites, boreal forests, midlatitude dry and humid climates [*Eck et al.*, 1999; *Holben et al.*, 2001; *Tanre et al.*, 2001; *Dubovik et al.*, 2002a; *Smirnov et al.*, 2002a], as well as their detailed description of daily to seasonal variations at specific sites such as the Canary Islands [*Smirnov et al.*, 1998], sub-Sahel West Africa [*Pinker et al.*, 2001], the Maldives [*Eck et al.*, 2001], and the Persian Gulf [*Smirnov et al.*, 2002b].

[4] Similar measurements, though still limited in duration and coverage, are emerging for the Mediterranean region. Sde Boker, in the Negev Desert of Israel, is the longest running station [*Ichoku et al.*, 1999; *Formenti et al.*, 2001a, 2001b; *Andreae et al.*, 2002]. Other relevant studies have been based on short-term dedicated field campaigns conducted at Crete and in the Aegean Sea [*Kouvarakis et al.*, 2002; *Sciare et al.*, 2002; *Formenti et al.*, 2002a, 2002b; *Bardouki et al.*, 2003], and Sun photometer measurements at several North African and coastal sites around the central and western Mediterranean Sea [*Masmoudi et al.*, 2003a, 2003b]. The present study complements these efforts by means of continuous surface-based Sun photometer measurements at a coastal site along the northeastern Mediterranean. All aerosol optical data from the region, when pooled together, provide a database which will allow improvements in the regional dust correction algorithm [*Moulin et al.*, 2001a, 2001b]. A brief overview of the data collection and retrieval procedure for the sun/sky radiance measurements are presented in section 2. Section 3 provides background information on general characteristics of Saharan dust transport over the Mediterranean. Regional aerosol optical characteristics are described in section 4. They include the monthly variations of aerosol optical thickness and Ångstrom coefficient for identification of major dust outbreaks (section 4.1), and an in-depth analyses of some specific events (section 4.2). Conclusions are given in section 5. Complementary information on aerosol chemical composition at the measurement site and some aspects of regional meteorological conditions can be found in *Kubilay and Saydam* [1995], *Kubilay et al.* [2000, 2002], *Özsoy et al.* [2000, 2001].

2. Data Collection and Retrieval

[5] Optical properties of aerosols were measured at the campus of Institute of Marine Sciences (IMS) of the Middle East Technical University (METU) near the rural town of Erdemli, situated along the southeastern coast of Turkey at 36°33′N and 34°15′E. This site is known as the IMS-METU-ERDEMLI site in the AERONET program. The measurements described in the present work cover a 17 month monitoring period starting at the begining of January 2000 and terminating in mid-June 2001, and were acquired by the CIMEL Sun photometer. The details of instrumentation, data acquisition and retrieval procedures have been described previously by *Holben et al.* [1998], *Dubovik and King* [2000], and *Dubovik et al.* [2000]. A brief description is, however, provided here for completeness. The direct sun radiance measurements were repeated every 15 min by the automatically tracking radiometer at four spectral bands (440, 675, 870, and 1020 nm). The sky radiance almucantar measurements were also acquired at these four spectral bands. Observations were then transmitted near-real time via satellite to the Goddard Space Flight Center, Maryland in the USA, where they were processed following the methodology of *Dubovik and King* [2000]. The daily mean values of the aerosol optical thickness (AOT), the Ångstrom coefficient (AC), the single-scattering albedo (SSA), and real and imaginary parts of the refractive index (REFR, REFI) were then retrieved at these four wavelengths. The total uncertainty in AOT measurements, being slightly higher in the UV wavelengths, is of the order of ±0.02, which is around 10% of typical aerosol loading with AOT $\sim$ 0.2. For desert dust loading with AOT(440nm) > 0.5, the accuracies are SSA $\sim$ 0.03, REFR $\sim$ 0.04 and REFI $\sim$ 40% [*Dubovik et al.*, 2000]. The accuracy levels drop down to SSA $\sim$ 0.05–0.07, REFR $\sim$ 0.05 and REFI $\sim$ 80–100% at lower desert dust loading characterized by AOT(440nm) < 0.2. Therefore the accuracy of AERONET retrieval decreases for low-aerosol loading; the most serious error is introduced for imaginary (absorption) part of the refractive index, which might however be reduced, to some extent, according to the intercalibration procedure suggested by *Kaufman et al.* [2002b]. The error in particle volume size distribution remains within 10% of the maxima, and 35% for minimum values for intermediate size range from 0.1 to 7.0 μm. The error, however, rises up to 80% for particle sizes smaller than 0.1 μm or larger than 7.0 μm [*Dubovik et al.*, 2000, 2002a]. Moreover, extensive testing of the inversion algorithm [*Dubovik et al.*, 2000] has shown the sensitivity of AERONET retrievals to dust particle nonsphericity. The assumption of nonsphericity was reported to generate higher concentrations of very small particles with radius less than 0.1 μm, as well as stronger spectral dependence of the real part of the refractive index. A new, revised retrieval algorithm [*Dubovik et al.*, 2002b] eliminates most of these artifacts, and will be incorporated in our future studies. Following the observations by *Tanre et al.* [2001], the choice of the algorithm is not critical in the present study, since we deal with specific dust events dominated by particles on the order of 1 μm or higher and by the AOT values greater than 0.5.

[6] Air mass back trajectories (72 hours), provided by the European Center for Medium Range Weather Forecasts (ECMWF), were utilized to show transport routes of air masses ending at 1000, 850, 700, and 500 hPa pressure levels at the sampling site. They were complemented by aerosol index data provided by the Earth Probe/Total Ozone

Mapping Spectrometer (EP/TOMS) and are utilized to designate the specific dust sources around the eastern Mediterranean during specific dust outbreak events [*Herman et al.*, 1997; *Torres et al.* 1998].

3. General Characteristics of Desert Dust Transport Over the Mediterranean Sea

[7] An extensive number of studies [*Moulin et al.*, 1998; *Kubilay et al.*, 2000; *Özsoy et al.*, 2001; *Israelevich et al.*, 2002, and references therein] have described the way in which desert dust from North Africa (i.e., Sahara desert) is transported over the Mediterranean. *Moulin et al.* [1998] identified three basic modes of dust transport over a year depending on the major paths of travelling cyclones. Spring months were shown to be generally characterized by the formation of the so-called Sharav cyclones along North Africa from its western to eastern boundaries. These cyclones are principally formed by differential heating between relatively colder oceanic waters to the north and warmer landmasses to the south. They then prefentially travel east-northeastward mobilizing massive amounts of Saharan dust into the eastern Mediterranean atmosphere [*Alpert and Ziv*, 1989]. The frequency and intensity of eastward travelling cyclones gradually reduces in the summer months as those developing in the western part of the Sahara are blocked by high-pressure systems over Libya (central North Africa). The associated dust transport is then preferentially oriented toward the central and western Mediterranean [*Martin et al.*, 1990; *Moulin et al.*, 1998]. Therefore only those cyclones from the eastern-Sahara provide mineral dust to the eastern Mediterranean atmosphere by low-level southerly transports. As southerly transports continue to supply desert dust to the eastern Mediterranean atmosphere in autumn, the development of low pressures near the Balearic Islands on the western side of North Africa direct the major pathway of dust transport toward the western Mediterranean. Less frequent dust transport events from Middle Eastern sources are also encountered in the region during the autumn [*Dayan et al.*, 1991; *Kubilay et al.*, 2000]. The impact of dust transport to the Eastern Mediterranean region greatly diminishes in winter principally due to frequent precipitaion in the region.

[8] The four year mean aerosol dust distribution inferred by TOMS aerosol index data from August 1996 to April 2000 [*Israelevich et al.*, 2002] suggests that the whole Northern African atmosphere is permanently loaded with significant amounts of desert dust during April–August. The highly energetic Sharav cyclones easily mobilize dust, and transports it eastward along the Mediterranean basin with a typical speed of 7–8 degrees of longitude per day, particularly during the spring months. The Saharan dust supply generally continues until the end of August with decreasing intensity and frequency. A very similar seasonal structure was also reported by the analysis of daily Meteosat visible images during 1994 [compare *Moulin et al.*, 1998, Figure 2]. The 33 yearlong climatological data along the coast of Israel in the eastern Mediterranean also supports the maximum occurence of Saharan dust events in the spring months [*Ganor*, 1994].

[9] Our findings for the years 2000 and 2001 also support this general picture of dust transport. In spring, the northeastern Mediterranean tends to receive dust supplies from the entire Saharan desert. The dust outbreaks then mainly originate from the central-eastern Sahara in summer, and the Middle East-Arabian peninsula in autumn. Contributions from urban-industrial aerosol intrusions into the region from the Eastern Europe, Balkan area, and Anatolia also prevail during summer-autumn months. Some examples of these cases are provided in the following section.

4. Aerosol Optical Properties at Erdemli

4.1. Seasonal-to-Daily Variations

[10] The seasonal variation of monthly mean AOT at the wavelength of 870 nm (Figure 1a) exhibited a bimodal Gaussian distribution with relatively higher values during the warmer half of the year. The primary peak (0.29 ± 0.32) occurred in April, the secondary peak (0.20 ± 0.12) in August, and AOT gradually decreased after September toward minimum values of around 0.10 in winter months (December, January, February). A similar trend was also observed for their standard deviations; high mean values were generally associated with similarly high-standard deviations, suggesting strong day-to-day variations in aerosol loading. Such variations were particularly apparent in April due to changes in the intensity and frequency of dust transport, variations in air mass trajectories transporting aerosols from different source regions (primarily North Africa, Middle East and continental Europe and Anatolian peninsula) to the measurement site, as well as changes in the wet and dry depositions associated with local meteorological conditions.

[11] The pronounced short term temporal variability of AOT at the wavelength of 870 nm during both 2000 and 2001 for the spring months is depicted more clearly in Figure 1b. The peaks of the order of 1.0 and even higher up to 1.85 observed during April 2000 signify short-lived intense dust storms. The predominance of large mineral dust particles characterizing these particular storms is supported by the corresponding Ångstrom coefficient (AC) values as low as $\sim$0.25, computed from the AOT measurements at 870 and 440 nm. Such distinct spring dust transports originate from low-level cyclogenesis taking place over North Africa. High winds and strong convective processes cause lifting of mineral dust particles into the atmosphere, which are then transported along the route of cyclones toward the northeastern Mediterranean, as suggested by air mass back trajectory analyses described in the next section. The secondary dust-dominated aerosol loading during summer months, suggested by somewhat higher AC values of 0.75–1.0, reflects a more heterogeneous vertical structure formed by different layers of mineral dust and other marine biogenic emissions and urban/industrial aerosol particles present at different altitudes; an example of which is also presented in the next section. Dust dominated aerosol events over Erdemli are observed less frequently during autumn and early winter months.

[12] The Ångstrom coefficient versus AOT plot given in Figure 1c indicates three different modes of aerosols. Mode 1 identified by large AOT (>0.5) and low AC (<0.5) values represent the strong spring desert dust transport events mainly from North Africa. Mode 2 yields essentially summer-time dust transports with AOT values varying between 0.20 and 0.50. These events are dominated either by

relatively coarse particles of dust with AC < 1.0 (Mode-2A), or by fine particles from other sources with AC > 1.0 (Mode-2B). Mode 3 represents the background aerosol content with AOT < 0.20 dominated mainly by fine particles (AC > 1.0) from anthropogenic, biogenic and biomass combustion aerosols. The prevailing contribution of fine particles to the summer period aerosol optical thickness (i.e., Mode 2B) is also suggested by the primary monthly mean AOT peak at the wavelength of 440 nm in August (Figure 1d).

4.2. Selected Dust Outbreak Episodes

[13] In order to illustrate in more detail the impacts of dust outbreaks from distinctly different sources on eastern Mediterranean aerosol optical properties, three dust intrusion events are presented. The event taking place in April 2000 is representative of "intense" dust transport from the Saharan desert. The October 2000 dust event provides an example of a "moderately strong" dust intrusion derived from the Middle East-Arabian peninsula. The August 2000 event, on the other hand, reflects a temporal accumulation of more heterogeneous aerosol material comprising Saharan and Middle East dust inputs as well as urban-industrial aerosol material from the north, i.e., the Balkans, Ukraine and Anatolia. The most pronounced daily aerosol optical thickness peaks characterize these three events, as indicated in Figure 1b by arrows, for the year 2000.

4.2.1. April 2000: An Intense Saharan Desert Dust Event

[14] The event in April represents one of the heaviest dust incursions encountered during the measurement period. The TOMS aerosol index distribution together with three-day back trajectory analysis suggested initiation of dust mobilization from western-central Sahara by 29 March (Figure 2a). A major cyclonic dust storm then started supplying Saharan dust from northern Libya and Egypt to the eastern Mediterranean atmosphere at levels from 1000 to 500 hPa (Figures 2a–2c). The TOMS aerosol index distribution for 31 March 2000 (Figure 2e) indicated that considerable dust mobilization had already took place in the region associated with this particular cyclonic activity. The depression then passed through the measurement site toward the Middle East during 2–3 April. Thus dust supply from the Middle East also contributed to the dust accumulation in the region (Figure 2d). Figure 3a illustrates the spectral aerosol optical depth variations during this particular heavy dust episode. On March 30, the background AOT values of around 0.2 started increasing to about 1.30 on 1 April and 1.85 on April 3. Dramatic changes of the Ångstrom coefficient values from >1.30 down to 0.07 (Figure 1b) together with neutral spectral dependence of AOTs on 2–3 April (Figure 3a) indicated the composition of this dense dust cloud with coarse particles larger than ~1 μm (Figure 3c).

[15] Single scattering albedo (SSA) was subject to considerable changes during the dust event (Figure 3b). Values around 0.90 (with slightly higher values at shorther wavelenths) prior to its initiation increased up to 0.97 (with

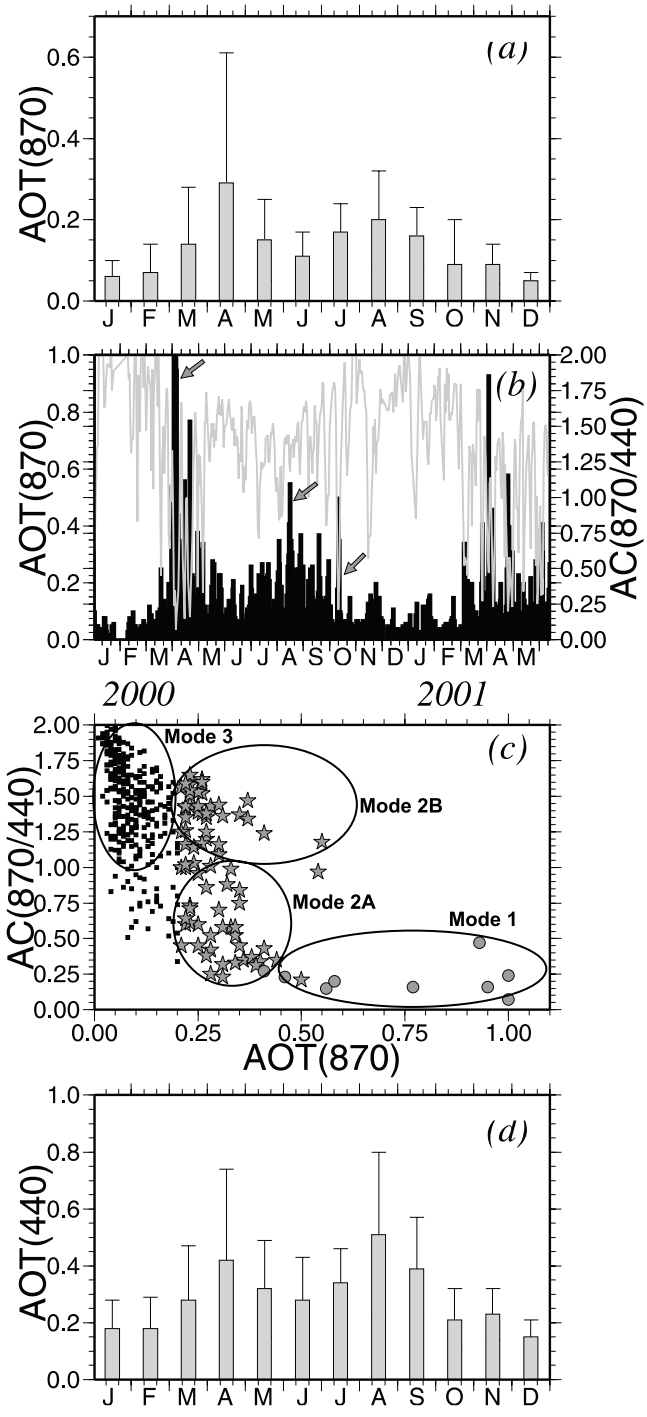

Figure 1. (opposite) (a) Variations of monthly average aerosol optical thickness at the wavelength of 870 nm with error bars showing one standard deviation, (b) time series plots of daily average aerosol optical thickness at 870 nm (bars) and Ångstrom coefficient computed using the wavelengths at 870 and 440 nm for the entire data set from 1 January 2000 to 15 June 2001, (c) scatter diagram of Ångstrom coefficient versus aerosol optical thickness, and (d) variations of monthly average aerosol optical thickness at the wavelength of 440 nm with error bars showing one standard deviation. Different symbols in Figure 1c correspond to the different aerosol modes signifying strong spring Saharan dust intrusions (dots), weak-to-moderately strong summer dust intrusions (stars), and background aerosols in the absence of any aerosol intrusion event (squares).

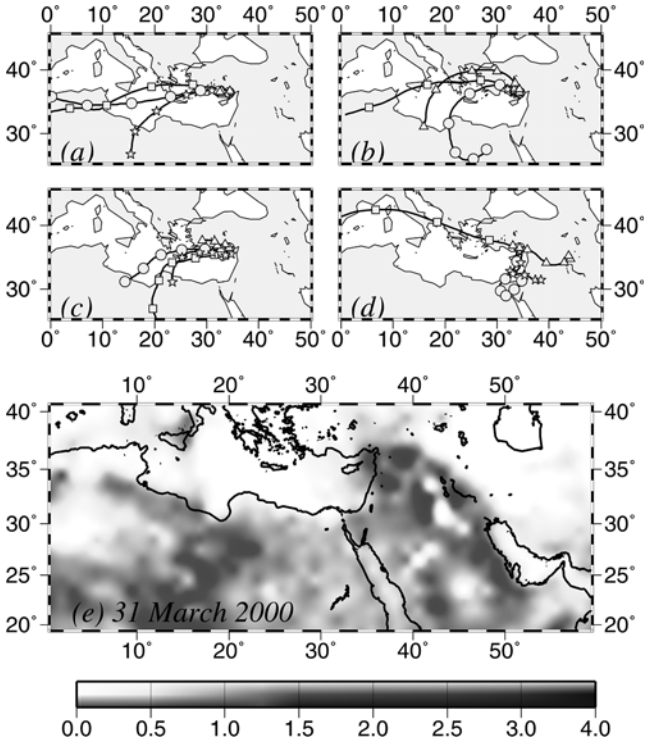

Figure 2. The three-day back trajectories showing the transport of air masses to the sampling site during (a) 29 March 2000, (b) 31 March 2000, (c) 1 April 2000, (d) 3 April 2000, and (e) regional aerosol index distribution on 31 March 2000. The back trajectory pathway every 12 hours is indicated by triangles for 1000 hPa, stars for 850 hPa, circles for 700 hPa and squares for 500 hPa.

slightly lower values at shorther wavelenths), being consistent with other values cited in the literature for desert dust [*Shettle*, 1984; *Pinker et al.*, 2001; *Dubovik et al.*, 2002a; *Smirnov et al.*, 2002b]. The SSA values then reduced around 0.90 at shorther wavelengths and below 0.90 at longer wavelengths following termination of the dust event. Relatively higher values at the time of the dust event were associated with their weak absorption (in other words, high-scattering) characteristics as compared to the aerosols from anthropogenic sources and biomass burning [*Dubovik et al.*, 2002a]. Moreover, SSA exhibited some wavelength dependence before and after this dust outbreak event; being lower at higher wavelengths, characteristic of both biomass burning and anthropogenically derived aerosols. In particular, the range of variations on 10 April, a week after the dust outbreak event, extended from 0.82 at 870 nm to 0.91 at 440 nm. Although not quite evident in our data, the available literature suggests an opposite wavelength dependence during desert dust episodes (higher values at longer wavelengths) due to the increased contribution of scattering from coarse dust aerosols [*Pinker et al.*, 2001; *Eck et al.*, 2001; *Dubovik et al.*, 2002a].

[16] Aerosol volume size concentration revealed two different types of distributions prior to and at the time of the outbreak event (Figure 3c). During 30–31 March, fine particles composed the major size group with radii between 0.06 and 0.6 μm, the majority concentrated around ~0.15 μm. The coarse fraction consisted of particles larger

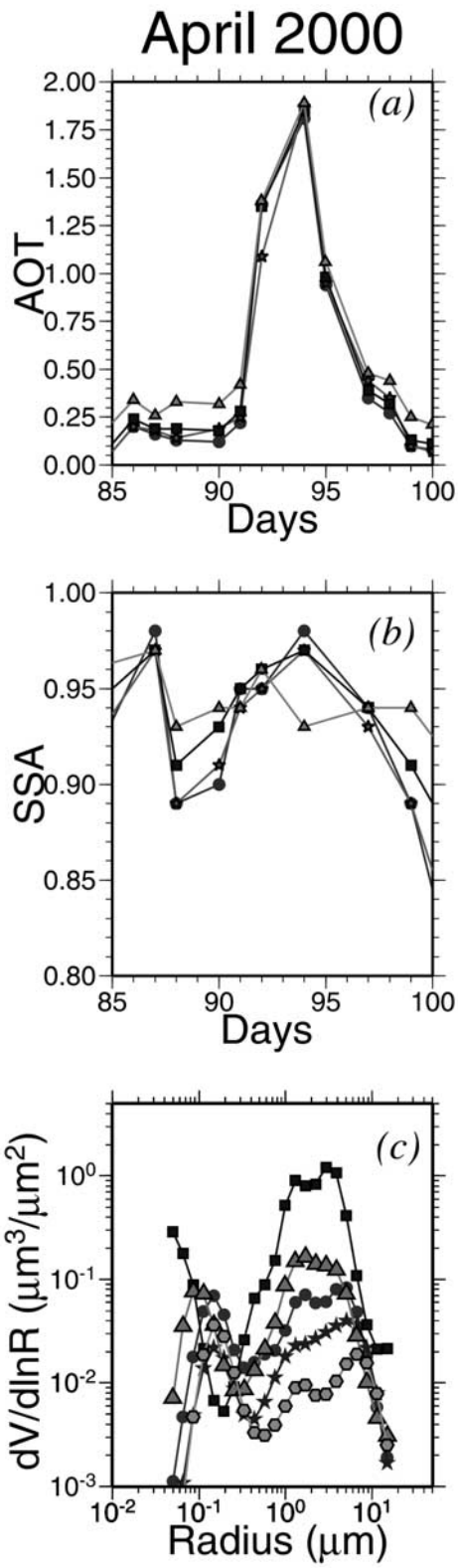

Figure 3. Time series plots for the (a) daily average values of aerosol optical thickness, (b) single scattering albedo between 25 March 2000 (Julian day 85) and 9 April 2000 (Julian day 100) at 440 nm (triangles), 670 nm (squares), 870 nm (stars), 1020 nm (dots), and (c) daily average aerosol volume size distributions for 31 March (stars), 1 April (dots), 3 April (squares), 6 April (triangles), and 10 April (hexagons).

Table 1. Indices of Refraction at Three Wavelengths (441, 673, and 873 nm) for Three Cases Representing an Event Prior to Dust Outbreak (31 March), During the Dust Break Event (3 April), and After the Termination of the Event (10 April)[a]

	31 March		3 April		10 April	
λ	$n(\lambda)$	$k(\lambda)$	$n(\lambda)$	$k(\lambda)$	$n(\lambda)$	$k(\lambda)$
441	1.33	1.93	1.44	1.91	1.36	2.03
673	1.34	2.08	1.58	1.12	1.40	2.34
873	1.36	2.43	1.59	1.03	1.44	3.02

[a]The variable $n(\lambda)$ denotes the real part representing scattering, and $k(\lambda)$ denotes the imaginary part representing absorbing and must be multiplied by 10^{-3}.

than 0.6 μm (up to 15 μm) with particle sizes mainly between ~1.0 μm and 6 μm. The columnar volume size concentrations for coarse and fine particles increased from 0.03 and 0.02 $\mu m^3\ \mu m^{-2}$, respectively, during 30 March to around 1.0 and 0.3 $\mu m^3\ \mu m^{-2}$ during 3 April, when a huge amount of desert dust accumulated at the measurement site. At the time of the dust outbreak, the coarse particle mode covered a broader size range larger than 0.2 μm with the major part of the columnar volume concentration formed by particles in the 1.0-to-5.0 μm size group. The volume concentration of the fine particle mode, on the other hand, was formed by particles with a radius of around 0.05 μm. Three-to-four days later, the volume size concentration of the coarse mode reduced an order of magnitude to values less than 0.15 $\mu m^3\ \mu m^{-2}$, and finally reverted back to background levels of 0.02 $\mu m^3\ \mu m^{-2}$ on 10 April, which is comparable to that prior to initiation of the dust outbreak event.

[17] The indices of refraction (with $n(\lambda)$ for scattering and $k(\lambda)$ for absorbing parts) at three wavelengths (440, 670 and 870 nm) prior to dust outbreak (31 March), during the dust break event (3 April), and after the termination of the event (10 April) are shown in Table 1. Before the intense desert dust loading, $n(\lambda)$ acquired its smallest values varying from 1.33 at 440 nm to 1.36 at 870 nm. When the site was influenced predominantly by coarse desert dust particles during 2–3 April, $n(\lambda)$ values increased at all wavelengths, from 1.44 at 440 nm to 1.59 at 870 nm due to more efficient scattering and less absorbing capabilities of the dust particles. Once dust-dominated coarse aerosols were withdrawn from the system, the scattering index attained pre-dust storm values. All values lie within the range of values 1.53 ± 0.05 reported for desert dust aerosols, and 1.39 ± 0.06 for urban-industrial dominated aerosols [*Dubovik et al.*, 2002a].

[18] The imaginary part of the refractive index, $k(\lambda)$, characterizes absorption of the medium, and varies over a wide range as a function of the mineralogy of the aerosols [*Sokolik and Toon*, 1999]. Generally speaking, pure desert aerosols are known to have very low absorption (in the visible) regardless of their sources as compared to highly absorbing urban aerosols. For the case of the April 2000 dust break event considered here, $k(\lambda)$ reduces from values of 0.002–0.003 prior to initiation and after termination of the desert dust loading to around 0.001 at the time of dust outbreak. Close similarity between these values indicates that atmospheric aerosols at the measurement site prior to the 2–3 April dust outbreak event should be dominated by a combination of low absorbing sea salt and dust particles as a remnant of previous events. Moreover, $k(\lambda)$ tends to increase (i.e., more absorption) at longer wavelengths before and after the dust event (which is typical for urban-industrial aerosols). The reverse relationship, holds at the time of desert dust intrusion, and $k(\lambda)$ decreases at longer wavelengths. These values lie within the range 0.0006–0.003 reported by *Dubovik et al.* [2002a] for different aerosol types measured at different regions.

4.2.2. October 2000: A Moderately Strong Desert Dust Event From the Middle East-Arabian Peninsula

[19] During October 2000 dust events, aerosols are primarily transported to the measurement site from the Middle East desert. The 3-day back trajectory analysis suggests eastward progression of a cyclonic system over Anatolia during the first week of October (Figure 4). The system traveled first in the northward direction (Figure 4a) and then veered gradually to the eastward direction during 1–4 October (Figure 4b), seems to give rise to only a limited aerosol loading from Anatolia at the measurement site. AOT was typically characterized by a value of 0.25 at 440 nm, and about 0.10 at higher wavelengths during this phase (Figure 5a).

[20] As the system was displaced further east, the mineral dust loading arrived from the Middle East and Arabian Peninsula during the subsequent two days (i.e., 5–6 October) preferentially between 1000–700 hPa, with some additional contribution from northwestern Africa at around

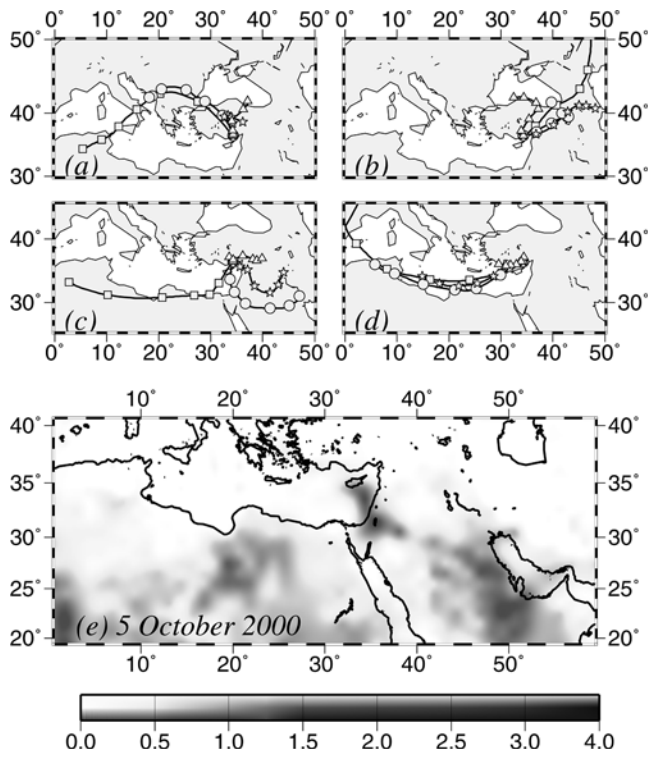

Figure 4. The three-day back trajectories showing the transport of air masses to the sampling site during (a) 1 October 2000, (b) 3 October 2000, (c) 6 October 2000, (d) 9 October 2000, and (e) the regional aerosol index distribution on 5 October 2000. The back trajectory pathway every 12 hours is indicated by triangles for 1000 hPa, stars for 850 hPa, circles for 700 hPa and squares for 500 hPa.

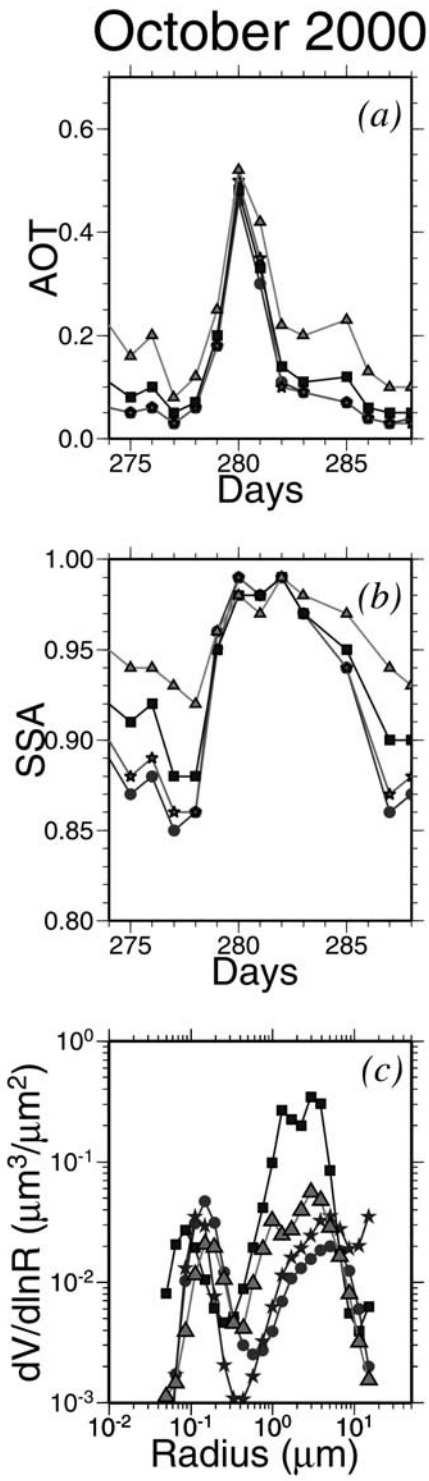

Figure 5. Time series plots for the (a) daily average values of aerosol optical thickness, (b) single scattering albedo between 30 September 2000 (Julian day 274) and 14 October 2000 (Julian day 288) at 440 nm (triangles), 670 nm (squares), 870 nm (stars), 1020 nm (dots), and (c) daily average aerosol volume size distributions for 2 October (dots), 4 October (stars), 6 October (squares), 8 October (triangles).

500 hPa level (Figure 4c). These two separate source regions are depicted in Figure 4e by the TOMS aerosol index distribution. Subsequently, the region is influenced at all levels by westerly air masses over the Mediterranean during the following few days (Figure 4d). The desert dust supply during 5–6 October caused an increase in AOT up to about 0.50, and a corresponding reduction in AC from 1.5 to 0.21 (cf. Figure 1b). Both AOT and SSA did not possess any appreciable wavelength dependence during this period. The weakly absorbing and strongly scattering character of the Middle East desert dust was noted by an increase of SSA up to 0.99 from its values of 0.93 at 440 nm and 0.85 at 870 nm on 4 October prior to the dust outbreak event (Figure 5b). SSA values reverted back to their pre-dust levels immediately after termination of the dust event.

[21] The scattering part of the refractive index attained values of about 1.50 during the dusty period, as compared to slightly lower values around 1.35–1.40 in the absence of a dust intrusion (Table 2). While these values are similar to those of the April 2000 case (cf. Table 1), the absorbing part of the refractive index reveals a greater range of variability from 0.0005 during the dusty period up to 0.005 ± 0.001 (signifying urban aerosol type) prior to dust outbreak event (Table 2). The absorption index value of 0.0005 is smaller than those of 0.0015 ± 0.0005 reported for the April 2000 Saharan dust event. The value of 0.0005 is in fact the default minimum value set in the algorithm [*Dubovik et al.*, 2000] as a value indistinguishable from absolute zero [*Kaufman et al.*, 2001]. Given the error range of 50–80% for the imaginary part of the refractive index, and of 0.03–0.04 for SSA at AOT > 0.5 at all wavelengths (cf. Section 2), it is thus possible to state that the difference between 0.0005 and 0.0015 is a geniune feature, and reflect different mineralogical character of the North Africa and Middle East desert dusts [*Sokolik and Toon*, 1999; *Caquineau et al.*, 2002].

4.2.3. August 2000: The Mixed Aerosol Event

[22] The third category of dust event is exemplified by an occurrence taking place during 10–12 August 2000. This event was characterized by variable aerosol intrusions at different altitudes. During 2–8 August, the dominant airflow into the region was directed from the north over the Ukraine, the Black Sea and Anatolia at all levels (Figures 6a and 6b). Northerly flow in the lower troposphere is a typical feature of this season, and is induced by a strong east-west pressure gradient between the quasi-permanent Azor high and Asian low-pressure systems. At the upper levels, the prevailing winds may, however, occasionally switch to

Table 2. Indices of Refraction at Three Wavelengths (441, 673, and 873 nm) for Three Cases Representing an Event Prior to Dust Outbreak (4 October), During the Dust Break Event (6 October), and After Termination of the Event (9 October)[a]

	4 October		6 October		9 October	
λ	$n(\lambda)$	$\mathbf{k}(\lambda)$	$n(\lambda)$	$k(\lambda)$	$n(\lambda)$	$k(\lambda)$
441	1.37	4.27	1.47	0.5	1.34	1.12
673	1.39	5.03	1.50	0.5	1.34	1.24
873	1.43	6.12	1.51	0.5	1.35	1.34

[a]The variable $n(\lambda)$ denotes the real part representing scattering, and $k(\lambda)$ denotes the imaginary part representing absorbing and must be multiplied by 10^{-3}.

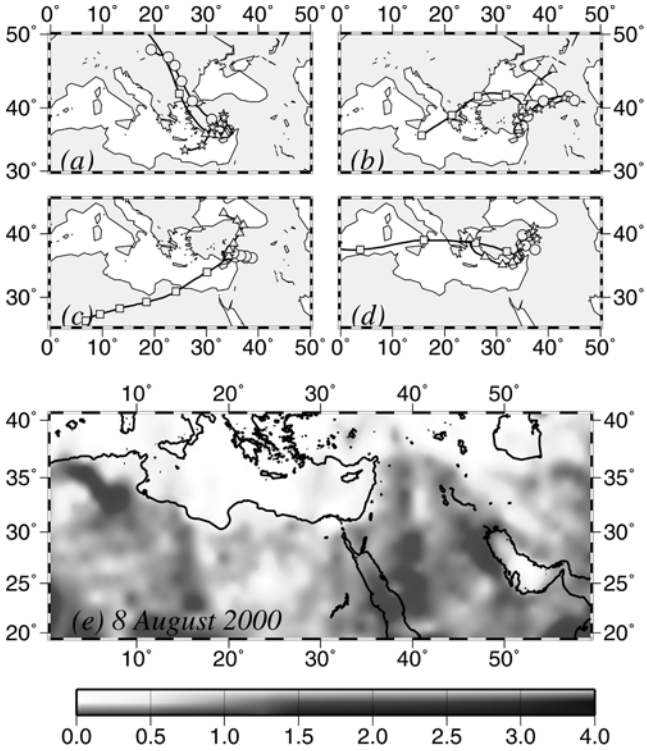

Figure 6. The three-day back trajectories showing the transport of air masses to the sampling site during (a) 2 August 2000, (b) 7 August 2000, (c) 12 August 2000, (d) 14 August 2000, and (e) the regional aerosol index distribution on 8 August 2000. The back trajectory pathway every 12 hours is indicated by triangles for 1000 hPa, stars for 850 hPa, circles for 700 hPa and squares for 500 hPa.

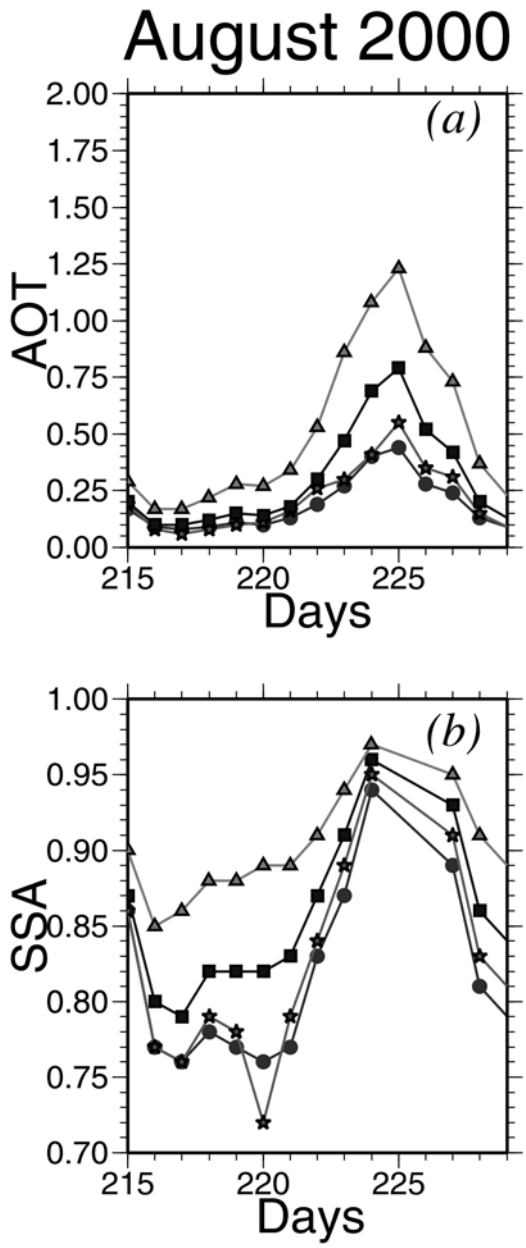

Figure 7. Time series plots for the (a) daily average values of aerosol optical thickness, and (b) single scattering albedo between 24 July 2000 (Julian day 207) and 16 August 2000 (Julian day 229) at 440 nm (triangles), 670 nm (squares), 870 nm (stars), 1020 nm (dots).

westerlies. The impact of such a flow system on the transport of air pollution during August 2001 has been recently studied by *Lelieveld et al.* [2002]. During 2–8 August 2000, this system was unable to introduce an appreciable dust loading to the measurement site as implied by low AOT values less than 0.25 and high AC values of ~1.40 (Figure 7a). Large spectral variability of SSA from 0.85–0.90 at 440 nm to 0.77–0.80 at 870 nm during this period (Figure 7b) as well as an order of magnitude higher values of the absorption index around 0.01 (Table 3) reflect the urban-industrial character of the dominant aerosols, with additional contributions from marine biogenic activities and forest fires in the region. Mixed nature of aerosol composition was independently confirmed by in situ chemical measurements conducted at various locations around the eastern Mediterranean [*Formenti et al.*, 2001a; *Sciare et al.*, 2002; *Kouvarakis et al.*, 2002; *Kubilay et al.*, 2002].

[23] The influence of an Azorean high-pressure system providing northerly air flow persisted near the surface during 9–12 August (see 1000 hPa trajectory in Figure 6c). The orientation of the flow at intermediate altitutes (shown by 850 and 700 hPa trajectories in Figure 6c), on the other hand, changed from north to southeast bringing dust into the region from the Middle East. At higher altitutes (see 500 hPa trajectory in Figure 6c) Saharan dust is transported toward the measurement site. These two specific dust sources are clearly evident in the TOMS aerosol index data (Figure 6e).

Table 3. Indices of Refraction at Three Wavelengths (441, 673, and 873 nm) for Three Cases Representing Prior to Dust Outbreak (5 August), During the Dust Break Event (11 August), and After Termination of the Event (16 August)[a]

	5 August		11 August		16 August	
λ	$n(\lambda)$	$k(\lambda)$	$n(\lambda)$	$k(\lambda)$	$n(\lambda)$	$k(\lambda)$
441	1.47	9.68	1.35	2.17	1.44	11.39
673	1.43	10.07	1.36	2.78	1.45	13.86
873	1.42	10.48	1.37	3.46	1.46	16.11

[a]The variable $n(\lambda)$ denotes the real part representing scattering, and $k(\lambda)$ denotes the imaginary part representing absorbing and must be multiplied by 10^{-3}.

The efficiency of this mechanism for changing the local aerosol optical characteristics was indicated by gradually increasing values of AOTs up to 0.54 at 870 nm and 1.25 at 440 nm, reduction of the Ångstrom coefficient to 1.18, an increase of the SSA values up to about 0.95, and reduction in the absorption index values to 0.002–0.003 on 11–12 August. The volume concentrations of both fine and coarse particles were about 0.10–0.15 $\mu m^3\ \mu m^{-2}$; the volume concentration of the coarse mode is therefore appreciably lower with respect to the previous two cases.

[24] Once high-level Saharan dust transport was terminated by the deflection of the 500 hPa air mass trajectory toward the north over the Mediterranean Sea during 13–14 August, the signature of the Saharan dust weakened at the measurement site. Similarly, the dust supply from the Middle East was terminated during the same period. Then, the aerosol optical characteristics once again reflected the urban-industrial signature; see, for example, changes in the absorption index values to the range of 0.011–0.016 during 16 August in Table 3, and decreases of single scattering albedo and AOT below 0.90 and 0.2, respectively.

5. Summary and Conclusions

[25] The aerosol optical measurement program recently initiated at a coastal rural site (IMS-METU-ERDEMLI) has provided a better understanding of dust optical characteristics in the northeastern Mediterranean. The study period extended from January 2000 to June 2001, and was characterized by frequent dust outbreaks from different sources around the region; with mineral dust being responsible for most of the variability in the aerosol optical properties. In particular, an increase in the volume concentration of coarse size particles was apparent, giving rise to more enhanced aerosol column extinction and light scattering, and reduced absorption at all wavelengths. The most intense dust events occurred during April for both 2000 and 2001. These dust events originated all over the Sahara and were transported to the measurement site at all altitudes. In summer and autumn months, long-range dust transport from the western-central sectors of North Africa are limited, and dust events generally occur at higher altitudes (700 hPa and higher) originating mainly from the nearby Middle East. Urban-industrial aerosols, advected at low-pressure levels (below 850 hPa) from Eastern Europe, the Balkan region and Anatolia by prevailing northerlies, introduced drastic changes for columnar optical characteristics depending on their relative contributions. When compared to the spring dust episodes, these events are identified by a lower aerosol optical thickness (<0.5), a higher Ångstrom coefficient (>1.0), higher absorption and an increased contribution of the fine mode to volume size spectra.

[26] The lack of a satisfactory database on optical properties of aerosols presents a major uncertainty in aerosol transport models, radiative forcing simulations and atmospheric retrieval and correction algorithms, particularly in regions around major dust sources, such as the eastern Mediterranean. For the first time, the present study reports a set of values as a source of input for these models and algorithms. The value estimated for the real part of refractive index under moderate-to strong dust event is 1.51 ± 0.07 at 440 nm, varying insignificantly with wavelengths. These values compare well with 1.55 ± 0.03 measured at Bahrain (Persian Gulf), 1.56 ± 0.03 at Solar-Vil (Saudi Arabia), and 1.48 ± 0.05 at Cape Verde [*Dubovik et al.*, 2002a]. For the imaginary part of the refractive index, our measurements suggest 0.0012 ± 0.0007 at 440 nm and 0.00075 ± 0.00025 at 870 nm. These values, however, vary to some extent depending on the origin of dust; Saharan dust has a higher absorbing and lower scattering signature as compared to that from the Middle East. The corresponding values at 440 nm are 0.0025 ± 0.001 at Bahrain, 0.0029 ± 0.001 at Solar Vil, and 0.0025 ± 0.001 at Cape Verde. The single scattering albedo values found in our measurements also fit into the range of values reported by *Dubovik et al.* [2002a]. Dust particles possess a bimodal size distribution with effective volume mean radii 2.2 μm and 0.08 μm for coarse and fine size fractions, respectively, with corresponding columnar volume size concentrations of about 1.0 and 0.1 $\mu m^3\ \mu m^{-2}$. The fine particle size distribution characteristics however may possess some error due to the sphericity assumption adopted in the inversion algorithm.

[27] **Acknowledgments.** This study was funded in part by METU Research Fund Project AFP-2001-07-01-01, the Turkish Scientific and Technical Research Council (TUBITAK) project 100Y121. We thank Brent Holben (NASA-GSFC) for providing us the Sun photometer within the framework of the AERONET program, the NASA/GSFC/TOMS group for the use of aerosol index data, and Emin Özsoy for making available the ECMWF trajectory analyses through collaboration with the Turkish State Meteorological Office. Technical assistance with the instrumentation, maintenance of the Sun photometer by Mehmet Demirel, and its calibration and processing of the data by the AERONET staff are greatly appreciated. We also thank Brent Holben, Oleg Dubovik as well as two anonymous referees for their insightful comments on the paper.

References

Andreae, T. W., M. O. Andreae, C. Ichoku, W. Maenhaut, J. Cafmeyer, A. Karnieli, and L. Orlovsky, Light scattering by dust and anthropogenic aerosol at a remote site in the Negev desert, Israel, *J. Geophys. Res.*, *107*(D2), doi:10.1029/2001JD900252, 2002.

Alpert, P., and B. Ziv, The Sharav cyclone: Observation and some theoritical considerations, *J. Geophys. Res.*, *94*, 18,495–18,514, 1989.

Bardouki, H., et al., Chemical composition of size-resolved atmospheric aerosols in the eastern Mediterranean during summer and winter, *Atmos. Environ.*, *37*, 195–208, 2003.

Caquineau, S., A. Gaudichet, L. Gomes, and M. Legrand, Mineralogy of Saharan dust transported over northwestern tropical Atlantic Ocean in relation to source regions, *J. Geophys. Res.*, *107*(D15), doi:10.1029/2000JD000247, 2002.

Claustre, H., A. Morel, S. B. Hooker, M. Babin, D. Antoine, K. Oulbelkheir, A. Bricaud, K. Leblane, B. Queguiner, and S. Maritorena, Is desert dust making oligotrophic waters greener?, *Geophys. Res. Lett.*, *29*(10), doi:10.1029/2001GL014056, 2002.

Dayan, U., J. Heffter, J. Miller, and G. Gutman, Dust intrusion events into the Mediterranean basin, *J. Appl. Meteorol.*, *30*, 1185–1199, 1991.

Dubovik, O., and M. D. King, A flexible inversion algorithm for retrieval of aerosol optical properties from Sun and sky radiance measurements, *J. Geophys. Res.*, *105*, 20,673–20,696, 2000.

Dubovik, O., A. Smirnov, B. N. Holben, M. D. King, Y. J. Kaufman, T. F. Eck, and I. Slutker, Accuracy assessments of aerosol optical properties retrieved from Aerosol Robotic Network (AERONET) Sun and sky radiance measurements, *J. Geophys. Res.*, *105*, 9791–9806, 2000.

Dubovik, O., B. N. Holben, T. F. Eck, A. Smirnov, Y. J. Kaufman, M. D. King, D. Tanre, and I. Slutsker, Variability of absorption and optical properties of key aerosol types observed in worldwide locations, *J. Atmos. Sci.*, *59*, 590–608, 2002a.

Dubovik, O., B. N. Holben, T. Lapyonok, A. Sinyuk, M. I. Mishchenko, P. Yang, and I. Slutsker, Non-spherical aerosol retrieval method employing light scattering by spheroids, *Geophys. Res. Lett.*, *29*(10), doi:10.1029/2001GL014506, 2002b.

Eck, T. F., B. N. Holben, J. S. Reid, O. Dubovik, A. Smirnov, N. T. O'Neill, I. Slutsker, and S. Kinne, Wavelength dependence of the optical depth of biomass burning, urban, and desert dust aerosols, *J. Geophys. Res.*, *104*, 31,333–31,349, 1999.

Eck, T. F., B. N. Holben, O. Dubovik, A. Smirnov, I. Slutsker, J. M. Lobert, and V. Ramanathan, Column-integrated aerosol optical properties over the Maldives during the northeast monsoon for 1998–2000, *J. Geophys. Res.*, *106*, 28,555–28,566, 2001.

Formenti, P., et al., Physical and chemical characteristics of aerosols over the Negev desert (Israel) during summer 1996, *J. Geophys. Res.*, *106*, 4871–4890, 2001a.

Formenti, P., et al., Aerosol optical properties and large-scale transport of air masses: Observations at a coastal and a semiarid site in the eastern Mediterranean during summer 1998, *J. Geophys. Res.*, *106*, 9807–9826, 2001b.

Formenti, P., et al., STAAARTE-MED 1998 summer airborne measurements over the Aegean Sea: 1. Aerosol particles and trace gases, *J. Geophys. Res.*, *107*(D21), 4450, doi:10.1029/2001JD001337, 2002a.

Formenti, P., et al., STAAARTE-MED 1998 summer airborne measurements over the Aegean Sea: 2. Aerosol scattering and absorption, and radiative calculations, *J. Geophys. Res.*, *107*(D21), 4451, doi:10.1029/2001JD001536, 2002b.

Ganor, E., The frequency of Saharan dust episodes over Tel Aviv, Israel, *Atmos. Environ.*, *28*, 2867–2871, 1994.

Gao, Y., Y. J. Kaufman, D. Tanre, D. Kolber, and P. G. Falkowski, Seasonal distributions of aeolian iron fluxes to the global ocean, *Geophys. Res. Lett.*, *28*, 29–32, 2001.

Hansen, J., M. Sato, R. Ruedy, A. Lacis, and V. Oinas, Global warming in the twenty-first century: An alternative scenario, *Proc. Natl. Acad. Sci. USA*, *97*, 9875–9880, 2000.

Heintzenberg, J., R. J. Charlson, A. D. Clarke, C. Liousse, V. Ramaswamy, K. P. Shine, M. Wendisch, and G. Helas, Measurements and modeling of aerosol single scattering albedo: Progress, problems and prospects, *Beitr. Phys. Atmos.*, *70*, 249–263, 1997.

Herman, J. R., P. K. Bhartia, O. Torres, C. Hsu, C. Seftor, and E. Celarier, Global distribution of UV-absorbing aerosols from Nimbus-7/TOMS data, *J. Geophys. Res.*, *102*, 16,911–16,922, 1997.

Holben, B. N., et al., AERONET-A federated instrument network and data archive for aerosol characterization, *Remote Sens. Environ.*, *66*, 1–16, 1998.

Holben, B. N., et al., An emerging ground-based aerosol climatology: Aerosol optical depth from AERONET, *J. Geophys. Res.*, *106*, 12,067–12,097, 2001.

Ichoku, C., M. O. Andreae, T. W. Andreae, F. X. Meixner, G. Schebeske, and P. Formenti, Interrelationship between aerosol characteristics and light scattering during late winter in an eastern Mediterranean environment, *J. Geophys. Res.*, *104*, 24,371–24,393, 1999.

Intergovernmental Panel on Climate Change, *Climate Change 2001*, *The Scientific Basis, Contribution of Working Group I to the Third Assessment Report of the Intergovernmental Panel on Climate Change*, Cambridge Univ. Press, New York, 2001.

Israelevich, P. L., Z. Levin, J. H. Joseph, and E. Ganor, Desert aerosol transport in the Mediterranean regions as inferred from the TOMS aerosol index, *J. Geophys. Res.*, *107*(D21), 4572, doi:10.1029/2001JD002011, 2002.

Kaufman, Y. J., D. Tanre, H. R. Gordon, T. Nakajima, J. Lenoble, R. Frouin, H. Grasll, B. M. Herman, M. D. King, and P. M. Teillet, Passive remote sensing of tropospheric aerosol and atmospheric correction for the aerosol effect, *J. Geophys. Res.*, *102*, 16,815–16,830, 1997.

Kaufman, Y. J., D. Tanre, O. Dubovik, A. Karnieli, and L. A. Remer, Absorption of sunlight by dust as inferred from satellite and ground-based remote sensing, *Geophys. Res. Lett.*, *28*, 1479–1482, 2001.

Kaufman, Y. J., D. Tanre, and O. Boucher, A satellite view of aerosols in the climate system, *Nature*, *419*, 215–223, 2002a.

Kaufman, Y. J., O. Dubovik, A. Smirnov, and B. N. Holben, Remote sensing of non-aerosol absorption in cloud free atmosphere, *Geophys. Res. Lett.*, *29*(18), doi:10.1029/2001GL014399, 2002b.

King, M. D., Y. J. Kaufman, D. Tanre, and T. Nakajima, Remote sensing of tropospheric aerosols from space: Past, present, and future, *Bull. Am. Meteorol. Soc.*, *80*, 2229–2259, 1999.

Kouvarakis, G., Y. Doukelis, N. Mihalopoulos, S. Rapsomanikis, J. Sciare, and M. Blumthaler, Chemical, physical, and optical characterization of aerosols during PAUR II experiment, *J. Geophys. Res.*, *107*(D18), 8141, doi:10.1029/2000JD000291, 2002.

Kubilay, N., and C. Saydam, Trace elements in atmospheric particulates over the Eastern Mediterranean; Concentrations, sources, and temporal variability, *Atmos. Environ.*, *29*, 2289–2300, 1995.

Kubilay, N., S. Nickovic, C. Moulin, and F. Dulac, An illustration of the transport of mineral dust onto the eastern Mediterranean, *Atmos. Environ.*, *34*, 1293–1303, 2000.

Kubilay, N., M. Koçak, T. Cokacar, T. Oguz, G. Kouvarakis, and N. Mihalopoulos, Influence of Black Sea and local biogenic activity on the seasonal variation of aerosol sulfur species in the eastern Mediterranean atmosphere, *Global Biogeochem. Cycles*, *16*(4), 1079, doi:10.1029/2002GB001880, 2002.

Lelieveld, J., et al., Global air pollution crossroads over the Mediterranean, *Nature*, *298*, 794–799, 2002.

Martin, D., G. Bergametti, and B. Strauss, On the use of the synoptic vertical velocity in trajectory model: Validation by geochemical tracers, *Atmos. Environ., Part A*, *24*, 2059–2069, 1990.

Masmoudi, M., M. Chaabane, D. Tanre, P. Gouloup, L. Blarel, and F. Elleuch, Spatial and temporal variability of aerosol: Size distribution and optical properties, *Atmos. Res.*, *66*, 1–19, 2003a.

Masmoudi, M., M. Chaabane, K. Medhioub, and F. Elleuch, Variability of aerosol optical thickness and atmospheric turbidity in Tunisia, *Atmos. Res.*, *66*, 175–188, 2003b.

Moulin, C., et al., Satellite climatology of African dust transport in the Mediterranean atmosphere, *J. Geophys. Res.*, *103*, 13,137–13,144, 1998.

Moulin, C., H. R. Gordon, V. F. Banzon, and R. H. Evans, Assessment of Saharan dust absorption in the visible from SeaWIFS imagery, *J. Geophys. Res.*, *106*, 18,239–18,249, 2001a.

Moulin, C., H. R. Gordon, R. M. Chomko, V. F. Banzon, and R. H. Evans, Atmospheric correction of ocean color imagery through thick layers of Saharan dust, *Geophys. Res. Lett.*, *28*, 5–8, 2001b.

Özsoy, E., N. Kubilay, S. Nickovic, and C. Moulin, A hemispheric dust storm affecting the Atlantic and Mediterranean (April 1994), Analyses, modelling, ground-based measurements and satellite observations, *J. Geophys. Res.*, *106*, 18,439–18,460, 2001.

Özsoy, T., C. Saydam, N. Kubilay, and I. Salihoglu, Aerosol nitrate and non-sea-salt sulfate over the eastern Mediterranean, *Global Atmos. Ocean Syst.*, *7*, 185–227, 2000.

Pinker, R. T., G. Pandithurai, B. N. Holben, O. Dubovik, and T. O. Aro, A dust outbreak episode in sub-Sahel West Africa, *J. Geophys. Res.*, *106*, 22,923–22,930, 2001.

Sciare, J., H. Bardouki, C. Moulin, and N. Mihalopoulos, Aerosol sources and their contribution to the chemical composition of aerosols in the eastern Mediterranean sea during summertime, *Atmos. Chem. Phys. Discuss.*, *2*, 1287–1315, 2002.

Shettle, E. P., Optical and radiative properties of a desert aerosol model, in *Proceedings of the Symposium on Radiation in the Atmosphere*, edited by G. Fiocco, pp. 74–77, A. Deepak, Hampton, Va., 1984.

Smirnov, A., B. N. Holben, I. Slutsker, E. J. Welton, and P. Formenti, Optical properties of Saharan dust during ACE 2, *J. Geophys. Res.*, *103*, 28,079–28,092, 1998.

Smirnov, A., B. N. Holben, Y. J. Kaufman, O. Dubovik, T. F. Eck, I. Slutsker, C. Pietras, and R. N. Halthore, Optical properties of atmospheric aerosol in maritime environments, *J. Atmos. Sci.*, *59*, 501–523, 2002a.

Smirnov, A., B. N. Holben, O. Dubovik, N. T. O'Neill, T. F. Eck, D. L. Westphal, A. K. Goroch, C. Pietras, and I. Slutsker, Atmospheric aerosol optical properties in the Persian gulf, *J. Atmos. Sci.*, *59*, 620–634, 2002b.

Sokolik, I. N., and O. B. Toon, Incorporation of mineralogical composition into models of the radiative properties of mineral aerosol from UV to IR wavelengths, *J. Geophys. Res.*, *104*, 9423–9444, 1999.

Tanre, D., Y. J. Kaufman, B. N. Holben, B. Chatenet, A. Karnieli, F. Lavenu, L. Blarel, O. Dubovik, L. A. Remer, and A. Smirnov, Climatology of dust aerosol size distribution and optical properties derived from remotely sensed data in the solar spectrum, *J. Geophys. Res.*, *106*, 18,205–18,217, 2001.

Tegen, I., A. A. Lacis, and I. Fung, The influence on climate forcing of mineral aerosols from disturbed soils, *Nature*, *380*, 419–422, 1996.

Torres, O., P. K. Bhartia, J. R. Herman, Z. Ahmad, and J. Gleason, Derivation of aerosol properties from satellite measurements of backscattered ultraviolet radiation: Theoretical basis, *J. Geophys. Res.*, *103*, 17,099–17,110, 1998.

Wang, M., S. Balley, and C. R. McClain, SeaWIFS provides unique global aerosol optical property data, *Eos Trans. AGU*, *81*(18), 197–202, 2000.

T. Cokacar, N. Kubilay, and T. Oguz, Institute of Marine Sciences, Middle East Technical University, Erdemli-Mersin, 33731, Turkey. (kubilay@ims.metu.edu.tr)